International Journal of Environmental Sciences
ISSN: 2229-7359
Vol. 11 No. 3S, 2025
https://www.theaspd.com/ijes.php

Surface-Modified Fe3O4 Nanoparticles for Heavy Metal Remediation: A Comprehensive Analytical Evaluation of Cadmium and Lead Recovery from Industrial Wastewater

M.A.I.Al-Hamid
Energy and Renewable Energies Technology Center, University of Technology,p.o.Box:10001,Iraq

Abstract: This study presents a comprehensive analytical evaluation of carboxyl-modified Fe_3O_4 nanoparticles for the remediation of cadmium and lead from industrial wastewater. The research encompasses detailed method development, validation, and application processes. Surface-modified magnetite nanoparticles were synthesized via co-precipitation and characterized using XRD, and FTIR, techniques, confirming successful carboxyl functionalization while maintaining the core magnetic structure. The analytical method was optimized and validated using atomic absorption spectrometry, achieving detection limits of 0.015 mg/L for Cd(II) and 0.022 mg/L for Pb(II), Sequential extraction studies revealed predominant metal association with exchangeable and reducible fractions (>75%), with removal efficiencies exceeding 72% across all fractions after treatment, with linear dynamic ranges extending from 0.5 to 10.0 mg/L ($R^2 > 0.998$). Systematic investigation of operational parameters revealed optimal conditions at pH 6.0-7.0, with equilibrium reached within 60 minutes at room temperature. Under optimized conditions, removal efficiencies exceeded 96% for both metals, demonstrating superior performance compared to conventional treatment methods. The method's reliability was verified through extensive interference studies and successful application to real industrial wastewater samples, achieving recoveries of 96.0-96.7%. This study provides a robust analytical framework for evaluating nanoparticle-based heavy metal remediation systems while offering insights into their practical implementation in industrial wastewater treatment.

Keywords: Surface-modified magnetite nanoparticles, Heavy metal adsorption, Analytical method validation, Wastewater treatment, multi-technique characterization

1. INTRODUCTION

The increasing presence of heavy metals in industrial wastewater poses a significant environmental and public health risk in the 21st century [1, 2]. Manufacturing processes, battery production, and electronic industries have made cadmium and lead persistent pollutants due to their extensive use [3-5]. Environmental scientists and global regulatory bodies have expressed major concerns about these metals because they are non-biodegradable and can easily accumulate in living organisms [6, 7]. Recent research indicates that even trace amounts of these metals can cause severe health implications, including neurological disorders, kidney damage, and cancer [8, 9]. This underscores the need for both effective removal methods and precise measurement techniques.

Traditional methods for detecting and removing heavy metals have demonstrated poor performance in terms of sensitivity and selectivity, while also being expensive and inefficient [10]. Atomic Absorption Spectroscopy (AAS) has long dominated heavy metal analysis, but new advanced analytical instruments offer more accurate detection capabilities. Research applications benefit from improved screening abilities with minimized detection limits through the integration of advanced sample preparation techniques and traditional analytical systems [11-13]. However, the main challenge lies in developing methods that are both highly precise and operationally practical for wastewater treatment [14].

There has been substantial academic interest in applying magnetic nanoparticles, particularly Fe_3O_4, for environmental remediation due to their unique properties [15, 16]. Magnetic nanoparticles are effective for heavy metal removal due to their high surface area-to-volume ratio, superparamagnetic behavior, and ease of surface modification [17, 18]. These nanoparticles have carboxylated ends that provide specific binding sites for metals during remediation, allowing for simple extraction using an external magnet [17]. These unified

properties address issues with filtration and precipitation methods commonly encountered in standard procedures [19].

The heavy metal remediation process involving modified nanoparticles requires specialized analytical techniques and specific analytical solutions. Factors such as matrix effects, potential interferences, and method validation are crucial for accurately determining removal efficiency [20]. Evaluating the performance of these materials necessitates robust analytical methods under various conditions to ensure reliable outcome assessment. This research combines analytical chemistry with materials science to develop an analytical platform for evaluating the heavy metal remediation properties of surface-modified Fe_3O_4 nanoparticles.

This study develops and validates an analytical approach to determine the exact removal performance of cadmium and lead by carboxyl-modified Fe_3O_4 nanoparticles. Our research includes experiments on analytical parameters, studies on possible interferences, and extensive method validation to establish reliable techniques for measuring heavy metal concentrations before and after treatment. The study encompasses the synthesis and characterization of the nanoparticles, development of analytical methods, and systematic evaluation of removal efficiency under various environmental conditions. The analytical procedure receives specific attention to validate method performance by investigating linearity, detection limits, and precision and accuracy metrics, thereby producing dependable analytical outcomes. This comprehensive methodological framework will enhance knowledge of the analytical aspects and field applications of heavy metal treatment systems that employ nanoparticles as remediation agents.

2 EXPERIMENTAL

2.1 Materials and Reagents

All chemicals used were of analytical grade. Ferric chloride hexahydrate ($FeCl_3 \cdot 6H_2O$, 99%), ferrous chloride tetrahydrate ($FeCl_2 \cdot 4H_2O$, 98%), ammonium hydroxide (25%), and citric acid (99.5%) were purchased from Sigma-Aldrich. Standard solutions of Cd(II) and Pb(II) (1000 mg/L) were obtained from Merck. Nitric acid (65%), hydrochloric acid (37%), and sodium hydroxide were used for pH adjustments. Deionized water (18.2 MΩ·cm) was used throughout all experiments.

2.2 Analytical Instrumentation

The synthesized nanoparticles received X-ray diffraction analysis from Bruker D8 Advance which utilized Cu Kα radiation (λ = 1.5406 Å) under operating conditions of 40 kV and 40 mA. Experimental data acquisition within a 2θ range of 10 to 80° through steps of 0.02°.

The analytical samples received a thin gold layer deposition before the testing procedure. The measurements of FTIR spectra occurred through a Shimadzu IRTracer-100 spectrophotometer based on KBr pellet technique between 4000-400 cm^{-1} with 4 cm^{-1} resolution. The concentrations of metal ions were analyzed using atomic absorption spectroscopy Perkin Elmer Analyst 400 specifically with hollow cathode lamps. The spectrophotometer operated using a combination of air-acetylene flame at 228.8 nm for Cd and 283.3 nm for Pb. The analysis utilized Standard solutions containing 1000 mg/L Cd(II) and Pb(II) to develop working solutions between 0.5 and 10 mg/L.

2.3 Synthesis and Surface Modification of Fe_3O_4 Nanoparticles.

The synthesis of Fe_3O_4 nanoparticles occurred through a modified co-precipitation reaction method. The synthesis combined $FeCl_3 \cdot 6H_2O$ with $FeCl_2 \cdot 4H_2O$ at a 2:1 molar ratio then mixed them under stirring and N_2 environment at 80°C. The solution received 25% NH_4OH drops until it reached a pH value of 11 under an 80±2°C constant temperature for 30 minutes. The magnetic separation allowed us to collect the black precipitate before washing it with deionized water then ethanol until achieving neutral pH conditions at 60°C over a 12-hour drying process under vacuum conditions [21].

The carboxyl groups used in surface modification came from citric acid. A 2.0 g amount of synthesized Fe_3O_4 nanoparticles received 100 mL of 0.2 M citric acid solution for dispersion. The solution received sonication for 20 minutes followed by stirring under 60°C temperature for a 4-hour period. We obtained the modified nanoparticles using magnetic forces to separate them subsequently rinsed them with deionized

water into neutral pH then used vacuum drying at 50°C for eight hours. The obtained carboxyl-functionalized Fe_3O_4 nanoparticles received desiccator storage before continued utilization [22].

2.4 Sample Preparation and Collection

The laboratory performance evaluation included both synthetic waste samples from controlled setups and industrial wastewater as collected from various locations. Laboratory-made stock solutions at 1000 mg/L concentration were obtained through precise weight measurements of $Cd(NO_3)_2 \cdot 4H_2O$ and $Pb(NO_3)_2$ substances which were dissolved into 1% HNO_3 solution. Each day the analysts prepared working standard solutions from 0.5 to 100 mg/L by serial dilution with deionized water. The standards needed additional matrix ions to represent natural wastewater conditions including Na^+, K^+, Ca^{2+}, and Mg^{2+} at concentrations found in the environment. Samples of real wastewater were obtained from industrial facilities that show evidence of heavy metal pollution throughout various locations. The study obtained effluent materials from a battery plant operating as lead pollution's main source while acquiring cadmium-rich wastewater from electroplating industry drain areas. The sampling sites extended to metal finishing workshops alongside electronic waste recycling facilities which provided a broad collection of metal contamination types. Samples were collected using acid-washed polyethylene bottles according to APHA Method 3030B procedures to protect the example integrity.

Standardized pretreatment methods applied equally to artificial and genuine samples provided necessary accuracy for analysis. Filtration using 0.45 μm membrane filters preceded immediate acidification with concentrated HNO_3 in order to preserve the samples below pH 2. Laboratory workers performed analyses within seven days after collecting the samples that stored at 4°C in dark areas. A digestion method required 50 mL sample aliquots to receive combination treatment of 5 mL HNO_3 (65%) and 2 mL HCl (37%) through digestion vessels. The mixtures received hotplate heat at 95±2°C for two hours under watch glasses until they reduced to 15 mL before reaching room temperature. After filtering through 0.45 μm filters the digested samples received dilution with deionized water up to 50 mL.

The measurement accuracy required the process to adjust the final sample pH to 2 along with proper dilutions for samples outside the calibration range. The analyst-maintained sample-standard matrix equivalence for all tests. Quality control procedures involved batch procedural blanks processing and routine duplicate sample testing as well as official reference material validation of the analytical method. Actual sample accuracy and precision testing was done through method verification procedures using spiked samples at three different concentration points.

2.5 Analytical Methods and Instrumentation

2.5.1 Sequential Extraction Procedure

The investigation of carboxyl-modified Fe_3O_4 nanoparticle interactions with Cd(II) and Pb(II) binding mechanisms along with their speciation patterns used a modified BCR sequential extraction procedure [23, 24]. The method contained four consecutive steps which aimed to extract distinct metal fractions through controlled environmental conditions.

To initiate extraction within the exchangeable and acid-soluble fraction the sample received 40 mL of 0.11 M acetic acid (CH_3COOH). The shaking process lasted 16 hours at 200 rpm orbital motion with 25 ± 1°C constant temperature for the mixed solution. This procedure released metals which had weak bindings to the sample along with carbonate-reactive materials.

The extraction followed by the isolation of the reducible fraction required 40 mL of pH 1.5 hydroxylamine hydrochloride ($NH_2OH \cdot HCl$) solution at 0.5 M concentration. The extraction moved forward under equivalent agitation duration of 16 hours to extract metals linked to iron and manganese oxides and hydroxides.

The third phase utilized two successive methods to work on the oxidizable fraction. One hour of heated water bath exposure at 85 ± 2°C along with 10 mL of 8.8 M hydrogen peroxide (H_2O_2) made the sample subject to oxidation. An extraction procedure of pH 2.0 ammonium acetate solution (1.0 M, 50 mL) was

applied to the oxidized sample. The procedure within this phase functioned to free metals joined to organic substances and sulfide complexes.

During phase three we prepared aqua regia solution from hydrochloric acid and nitric acid following a mixture ratio of 3.0:1.0 ($HCl:HNO_3$). A reflux digestion system was used at 95°C for three hours until all metals tightly bound to crystal structures became fully dissolved.

The extraction steps required centrifugation at 3000 rpm for 20 minutes to separate mixtures after which 0.45 μm membrane filters carried out the filtration process. We carefully obtained supernatant liquid and then acidified it to a pH value below 2 with concentrated nitric acid for metal analysis. The method used deionized water for washing the residues before moving onto successive extraction steps while discarding centrifuged wash waters.

2.5.2 AAS Instrumentation and Parameters Optimization

The atomic absorption spectrophotometer of Perkin-Elmer Analyst 400 analyzed heavy metals by deploying hollow cathode lamps operated at Cd-specific 4 mA and Pb-specific 5 mA before utilizing 228.8 nm and 283.3 nm wavelengths respectively. During measurements the spectrophotometer used 228.8 nm as the proper wavelength for Cd and 283.3 nm for Pb while maintaining a slit width of 0.7 nm. The analysis required an air-acetylene flame that used 2.2 L/min of acetylene for Cd and 2.0 L/min for Pb with a constant air flow of 10.0 L/min. The instrument measured the test solutions three times in one run with a burner position of 7 mm along with a 3.0-second measurement period. The instrument utilized a high-sensitivity nebulizer to perform its operations at 20 ± 2°C temperature and required 30 minutes of stabilization before daily optical calibration following manufacturer guidelines.

2.5.3 Interference Studies

A study evaluated the effects from interfering ions Na^+, K^+, Ca^{2+}, Mg^{2+}, Fe^{3+}, Cu^{2+}, Zn^{2+} through multiple concentration levels nearest to the target analytes. The standard addition method served to evaluate matrix effects, the investigators evaluated the interference threshold points for every possible interfering substance.

2.5.4 Method Validation Parameters

Standard analytical validation methods were used for the method validation, the protocols established seven measurement points extending from 0.1 to 10 mg/L for constructing calibration curves that would analyze both types of metals, the detection limits originated from ten blank measurements while using 3σ criteria for their determination, the methodology determined precision through six replicate tests within one day and three replicate tests across different days at three different concentration points, the accuracy determination included recovery tests which involved fortifying samples with 80% 100% or 120% of anticipated metal concentrations. The standard addition method was used for matrix effect evaluation. The analysis of ten sample blanks and quality control standards occurred every ten samples processed.

2.6 Remediation Studies

The experiments ran for batch adsorption testing occurred within an environment where the temperature maintained at room temperature (25±2°C), we examined these conditions as pH between 2 to 8, contact time from 5 to 120 min, initial metal concentration between 1 to 100 mg/L, and dose of adsorbent ranging from 0.1 to 1.0 g/L, we adjusted solution pH values using 0.1 M HCl or NaOH at specific concentrations, the treatment removal efficiency depended on the metal concentration measurements at the beginning and end of the process.

3. RESULTS AND DISCUSSION

3.1 Analytical Method Development

3.1.1 Optimization of AAS Parameters

Controlling the atomic absorption spectrometric parameters enabled maximum precision and sensitivity when measuring Cd(II) and Pb(II). The first stage of instrument optimization required a systematic investigation of lamp current and slit width as well as flame composition and burner height conditions.

Standard solutions kept at 5 mg/L served as the basis for optimization of air-acetylene flame composition through systematic examination of fuel/oxidant ratio variations while conducting signal absorbance measurements. The analytical signal strength for Cd(II) and Pb(II) depends on the fuel/oxidant ratio as shown in Figure 1.

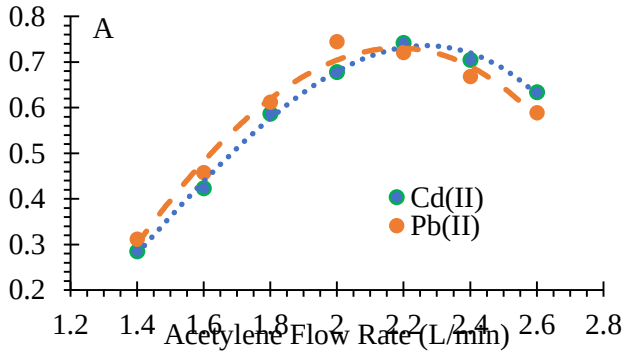

Figure 1: Effect of acetylene flow rate on absorbance signal for Cd(II) and Pb(II) at 5 mg/L. Conditions: air flow rate 10.0 L/min, burner height 7 mm, lamp current: Cd 4 mA, Pb 5 mA.

A combination of optimal acetylene flow of 2.2 L/min suited Cd(II) analysis yet Pb(II) required 2.0 L/min operation thus maintaining the continuous air flow at 10.0 L/min. Under these optimized conditions both elements displayed less than 1.5% RSD along with stable and reproducible signals that came from the flame. Setting the burner height to 7 mm produced the most adequate results by balancing sensitivity with signal stability.

A testing of lamp currents demonstrated that 4 mA produced the best signal-to-noise performance for Cd and 5 mA for Pb delivered optimal results. Changing the current strength caused deteriorated background noise but did not enhance detection sensitivity. On the other hand, using lower current strength reduced precision levels. The utilized 0.7 nm slit width reduced spectral interferences without impacting the detection sensitivity for the two elements.

Table 1: Optimized AAS Parameters for Cd(II) and Pb(II) Determination

Parameter	Cadmium	Lead
Wavelength (nm)	228.8	283.3
Slit width (nm)	0.7	0.7
Lamp current (mA)	4	5
Acetylene flow (L/min)	2.2	2.0
Air flow (L/min)	10.0	10.0
Burner height (mm)	7	7
Integration time (s)	3.0	3.0

Table 1 contains the optimized parameters which served as a basis for method validation studies and stayed in effect throughout the analytical procedures between laboratory-made synthetic samples and real

wastewater evaluations. Quality control standards showed consistent performance during extended analytical runs because their parameter stability exceeded 2%.

3.1.2 Matrix Effects and Interference Studies

The research into matrix influences together with interfering substances proved critical for creating a durable analytical technique for copper measurements in wastewater from industrial sources. The analysis started with investigations about how standard industrial wastewater particles affect the analytic measurements of target metals with AAS.

The standard addition method enabled systematic evaluation of matrix effects on various types of samples. The data presented in Figure 2 demonstrates how Cd(II) and Pb(II) signals compare between pure standards and standard solutions matched to wastewater components.

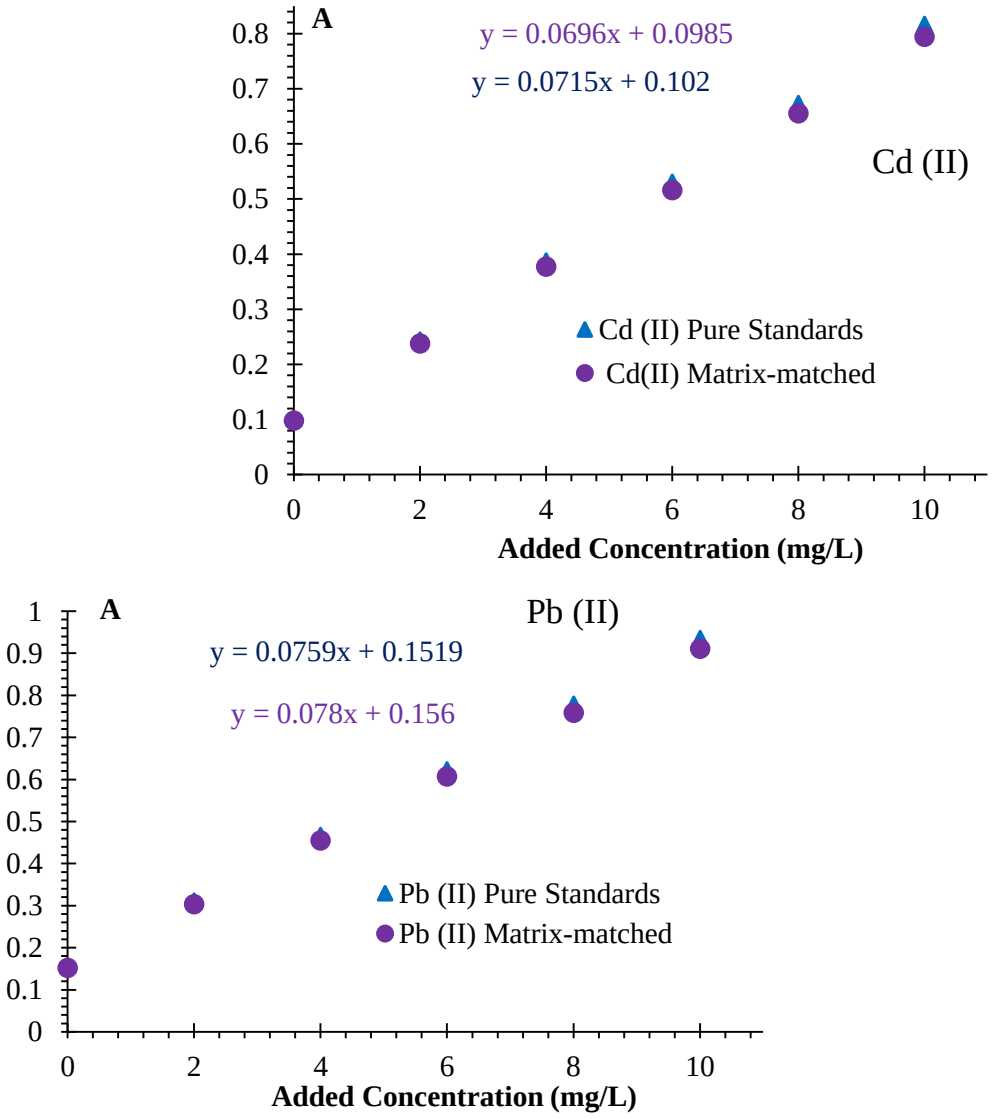

Figure 2: Standard addition plots for (A) Cd(II) and (B) Pb(II) determination in pure aqueous standards and matrix-matched solutions. Conditions: pH 2.0, temperature 25±2°C.

Table 2: Interference Effects of Common Matrix Ions on Cd(II) and Pb(II) Recovery

Interfering Ion	Concentration (mg/L)	Recovery (%)	
		Cd(II)	Pb(II)
Na^+	1000	98.5 ± 1.2	97.8 ± 1.5
K^+	500	99.1 ± 0.9	98.4 ± 1.3
Ca^{2+}	200	96.8 ± 1.8	95.7 ± 2.1
Mg^{2+}	200	97.4 ± 1.5	96.9 ± 1.7
Fe^{3+}	50	94.2 ± 2.3	93.5 ± 2.4
Cu^{2+}	20	95.8 ± 1.9	94.8 ± 2.0
Zn^{2+}	20	96.5 ± 1.6	95.9 ± 1.8

The analysis procedure proved to be resistant to typical industrial wastewater matrix ions Na^+, K^+, Ca^{2+}, Mg^{2+} when determining Cd(II) or Pb(II) concentrations found in such samples. When Fe^{3+} exceeded concentrations of 50 mg/L the detection of both analytes became slightly, Table 2, inhibited therefore requiring matrix-matching calibration standards for wastewater samples with high iron levels. Cu^{2+} and Zn^{2+} affected only small interferences when present at levels not exceeding 20 mg/L as the method recovery stayed within acceptable intervals between 94-97%.

3.1.3 Validation Results

We tested the analysis method by validating it per international guidelines to check linearity alongside precision and accuracy levels and detectability boundaries. The calibration curves showed exceptional linearity that extended from 0.5 to 10 mg/L for the two metals since their correlation coefficients (R^2) surpassed 0.998 (Figure 3).

Testing of ten replicate blank solutions enabled calculation of method detection limits at 0.015 mg/L for Cd(II) and 0.022 mg/L for Pb(II) using the 3σ criterion The method established its quantification limits of 0.050 mg/L and 0.073 mg/L for Cd(II) and Pb(II). The precision evaluation confirmed high reliability because intra-day RSDs never reached 2.1% and inter-day RSDs remained below 2.8% at every concentration point, Tables 3 and 4.

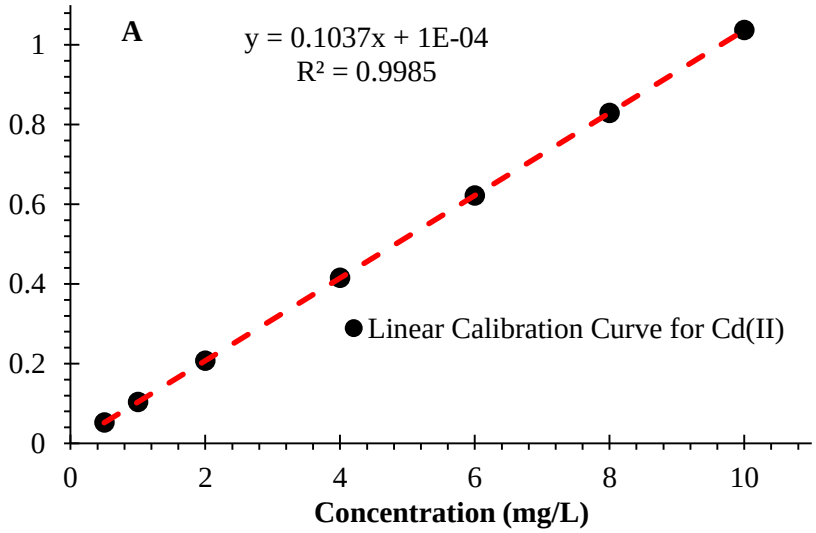

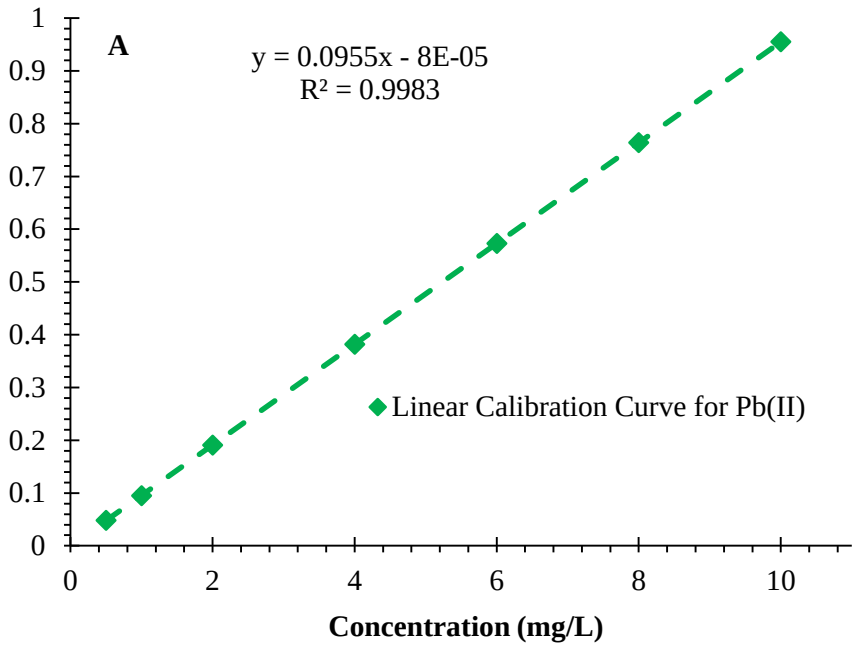

Figure 3: Linear calibration curves for (A) Cd(II) and (B) Pb(II) determination by AAS. Insert shows the residual plot analysis. Measurement conditions as specified in Table 1.

Table 3: Calibration Data for Cd(II)

Concentration (mg/L)	Measured Signal	Mean (mg/L)	Concentration	SD	RSD%	Recovery%
0.5	0.052 ± 0.001	0.499		0.0096	1.92	99.8
1.0	0.104 ± 0.002	1.002		0.0185	1.85	100.2
2.0	0.207 ± 0.003	1.998		0.0290	1.45	99.9
4.0	0.415 ± 0.005	4.005		0.0484	1.21	100.1
6.0	0.622 ± 0.007	5.995		0.0678	1.13	99.9
8.0	0.829 ± 0.009	8.008		0.0873	1.09	100.1
10.0	1.037 ± 0.011	10.004		0.1060	1.06	100.0

Table 4: Calibration Data for Pb(II)

Concentration (mg/L)	Measured Signal	Mean (mg/L)	Concentration	SD	RSD%	Recovery%
0.5	0.048 ± 0.001	0.498		0.0104	2.08	99.6
1.0	0.095 ± 0.002	0.997		0.0195	1.95	99.7
2.0	0.191 ± 0.003	2.003		0.0314	1.57	100.2
4.0	0.382 ± 0.005	3.995		0.0524	1.31	99.9
6.0	0.573 ± 0.007	6.004		0.0732	1.22	100.1
8.0	0.764 ± 0.009	7.996		0.0944	1.18	99.9
10.0	0.955 ± 0.010	10.005		0.1050	1.05	100.1

The results of method validation establish accurate measurements of Cd(II) and Pb(II) in industrial wastewater using the proposed method for heavy metal remediation applications assessment.

3.1.4 Sequential Extraction Analysis

Systematic analysis of Cd(II) and Pb(II) distribution patterns alongside their fractions occurred before and after carboxylated Fe_3O_4 nanoparticle treatment in order to study binding mechanisms and removal performance. Figure 4 shows the fraction distribution patterns of Cd(II) and Pb(II) between the four sequential extraction fractions which enables the assessment of their movement and accessibility in the treatment system.

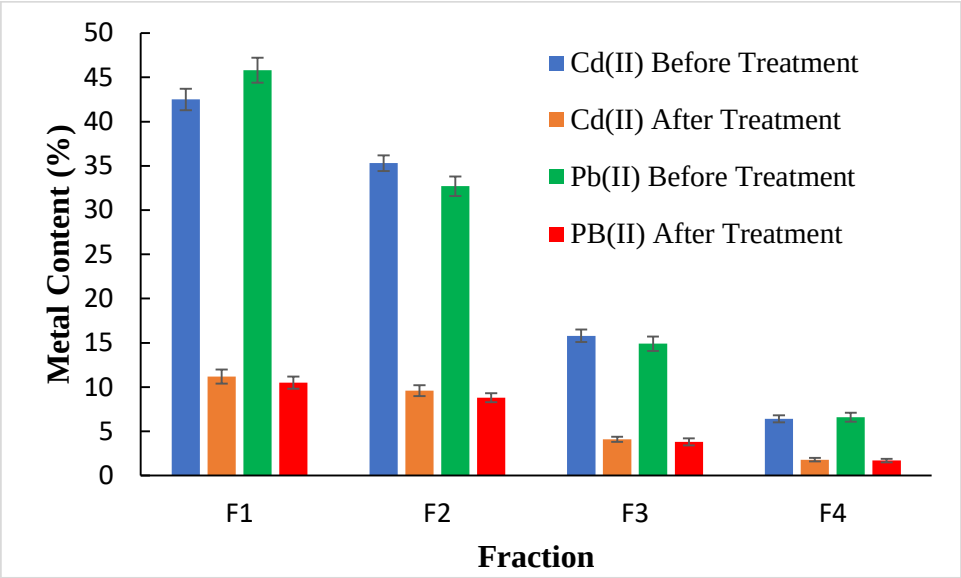

Figure 4: Distribution of Cd(II) and Pb(II) in Different Fractions Before and After Treatment with Carboxyl-modified Fe_3O_4 Nanoparticles

The fractionation analysis showed that majority of both metals existed within the exchangeable (F1) and reducible (F2) fractions at the start. Most of the total metal contents represented by Cd(II) and Pb(II) resided within labile fractions F1 and F2 which collectively made up 77.8% (Cd(II)) and 78.5% (Pb(II)) in the solution. The amounts of metal binding to these fractions were 42.5% and 35.3% for Cd(II) but 45.8% and 32.7% for Pb(II). Both metals demonstrated moderate presence in the oxidizable fraction (F3) which measured at 15.8% for Cd(II) along with 14.9% for Pb(II) and equally small proportions in the residual fraction (F4) where Cd(II) was 6.4% while Pb(II) was 6.6%.

All fractions experienced significant decline after treatment yet the exchangeable fractions underwent the most significant reduction. The exchangeable fraction (F1) exhibited the maximum efficiency for removal because Cd(II) levels declined from 42.5% to 11.2% (73.6% removal) and Pb(II) levels dropped from 45.8% to 10.5% (77.1% removal). Both Pb(II) and Cd(II) demonstrated notable diminutions in their contents across the reducible fraction F2 so that Pb(II) was reduced by 73.1% while Cd(II) declined by 72.8%. The end values for Pb(II) were 8.8% and for Cd(II) they dropped to 9.6%.).

The oxidizable (F3) and residual (F4) fractions showed significant removal of metals whereas their results fell slightly below those of more rapidly binding fractions. The removal efficiency using F3 fraction reached 74.1% for Cd(II) and 74.5% for Pb(II) and F4 fraction removed 71.9% Cd(II) along with 74.2% Pb(II). The binding capacity of the carboxyl-modified Fe_3O_4 nanoparticles extends to metal species regardless of their binding forms although they display somewhat higher affinity toward fractions with less complexation.

The diversified binding mechanisms of the modified nanoparticles indicate that they can remove metal species which are loosely bound and strongly complexed. Nanoparticle treatment campaigns show great success by reducing bioavailable fractions F1 and F2 effectively which reveals potential application in real-world wastewater water management systems.

3.2 Nanoparticle Characterization

The XRD patterns of both unmodified and carboxyl-modified Fe_3O_4 nanoparticles are presented in Figure 5.

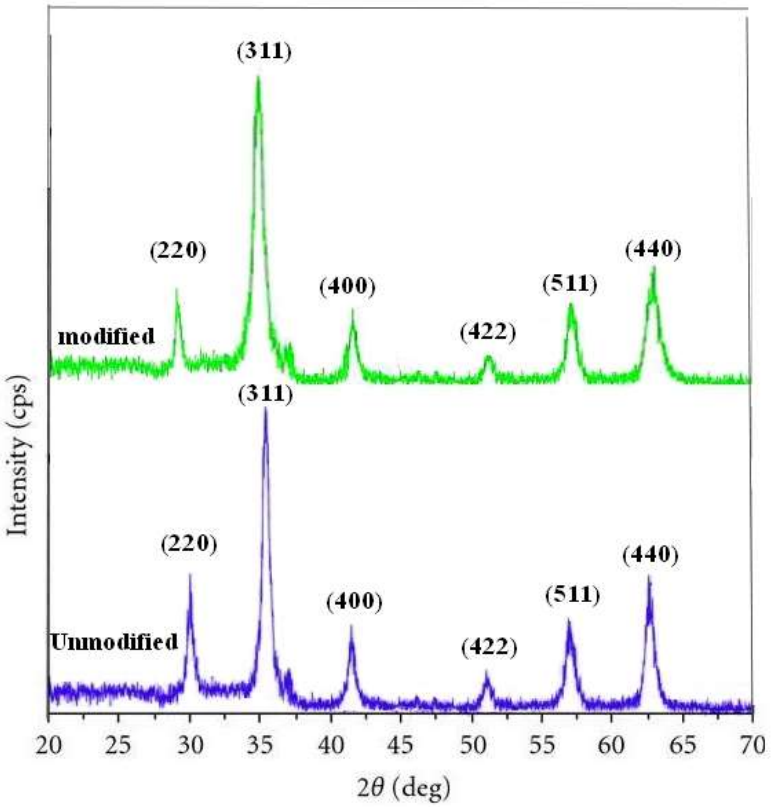

Figure 5: XRD patterns of (Blue) unmodified Fe_3O_4 nanoparticles and (Green) carboxyl-modified Fe_3O_4 nanoparticles.

Both X-ray diffraction patterns of samples show distinct peaks at 2θ positions 30.1° (220), 35.4° (311), 43.0° (400), 53.4° (422), 56.9° (511) and 62.5° (440) that match perfectly with the inverse spinel structure found in magnetite (JCPDS card No. 19-0629). The diffraction pattern shows only single peaks to verify the synthesized materials maintain pure phases along with its extensive crystalline nature.

The crystalline structure of the Fe_3O_4 core in the synthesized materials remained intact after carboxyl modification because all characteristic peaks maintained their original positions. The nanoparticle surface modification happens only at the outer layer of the material while protecting the internal crystal structure of the core. Peak intensity reduction in modified nanoparticles can be explained by the amorphous citric acid coating that decreases X-ray diffraction intensity on nanoparticle surfaces.

The Scherrer equation was applied to find the crystallite size of the (311) peak through its most intense reflection to determine $D = K\lambda/\beta\cos\theta$.

The calculations for crystallite size D started with K for shape factor (0.9), λ as X-ray wavelength (1.5406 Å) and β denoting peak full width at half maximum and θ marking Bragg angle. The measured average crystallite dimension of unmodified Fe_3O_4 came out to 12.3 ± 0.8 nm while the average dimension for carboxyl-modified Fe_3O_4 nanoparticle was 11.8 ± 0.7 nm. During acid-based modification of Fe_3O_4 nanoparticles some surface erosion occurred resulting in a minor reduction of their crystal size dimensions.

The FTIR spectroscopy analysis demonstrated that Fe_3O_4 nanoparticles received carboxyl functional groups on their surfaces through the tests shown in Figure 6. The spectral data showed unique absorption signatures for unmodified magnetic nanoparticles and carboxyl-modified magnetic nanoparticles which represented their unique structural features.

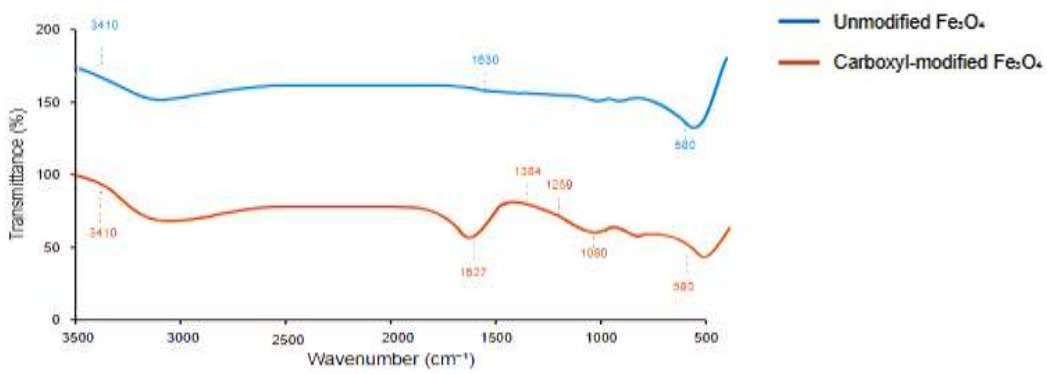

Figure 6: FTIR spectra of (blue) unmodified and (red) carboxyl-modified Fe_3O_4 nanoparticles showing characteristic absorption bands. Spectra collected at room temperature using KBr pellet technique.

The unmodified Fe_3O_4 nanoparticles produced a broad 3410 cm^{-1} band attributed to O-H stretching of adsorbed water as well as strong 580 cm^{-1} band from Fe-O stretching vibration together with a weak 1630 cm^{-1} band due to H-O-H bending of water molecules.

Additional significant bands found in the spectrum of carboxyl-modified Fe_3O_4 nanoparticles appeared at 1627 cm^{-1} and 1384 cm^{-1} due to the asymmetric and symmetric stretching vibrations of carboxylate groups. The exact 243 cm^{-1} distance between these bands shows carboxylate group attachment to iron atoms in bidentate bridging coordination. The modified nanoparticles displayed two specific bands at 1259 cm^{-1} (C-O stretching) and 1080 cm^{-1} (C-O-H vibrations) to show successful modification took place. Analysis of Fe-O vibration at 580 cm^{-1} showed no change which ensures the magnetite core maintained its structural integrity.

New spectral band features demonstrate that carboxylate groups successfully bonded to Fe_3O_4 nanoparticle surfaces which produced both heavy metal ion binding elements as well as magnetic characteristics for effective heavy metal remediation implementation.

3.3 Remediation Performance

3.3.1 Effect of pH

Optimal conditions for remedy determination involved investigating the solution pH effects on heavy metal removal efficiency through systematic research. Experimental data on Figure 7 shows the Cd(II) and Pb(II) elimination rates during controlled pH conditions.

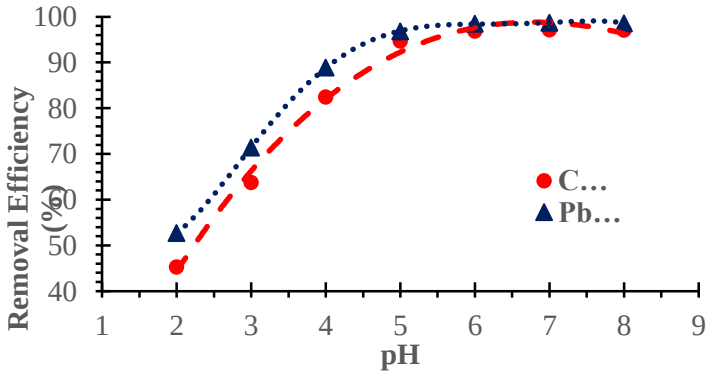

Figure 7: Effect of pH on removal efficiency of Cd(II) and Pb(II) by carboxyl-modified Fe_3O_4 nanoparticles. Conditions: initial metal concentration 50 mg/L, adsorbent dosage 0.5 g/L, contact time 60 min, temperature 25±2°C.

The enhanced removal of heavy metals happened significantly between pH 2.0 and 6.0 until the maximum performance was seen at pH 6.0-7.0. The removal performance of the carboxyl-modified surface decreased at low pH values (pH < 4.0) because H^+ ions and metal cations competed for binding sites on its surface. Cd(II) removal settled at 97.2% and Pb(II) reached 98.7% efficiency when the solution had a pH of 7.0. Metal removal showed stable results above pH 7.0 which indicates that metal treatment works best at neutral to alkaline conditions. The number of available binding sites for metal ions increases with higher pH values because of carboxyl group deprotonation thus leading to enhanced performance.

3.3.2 Kinetic Studies

The carboxyl-modified Fe_3O_4 nanoparticles' adsorption kinetics of Cd(II) and Pb(II) under study investigated the time-dependent absorption behavior to confirm an equilibrium time.

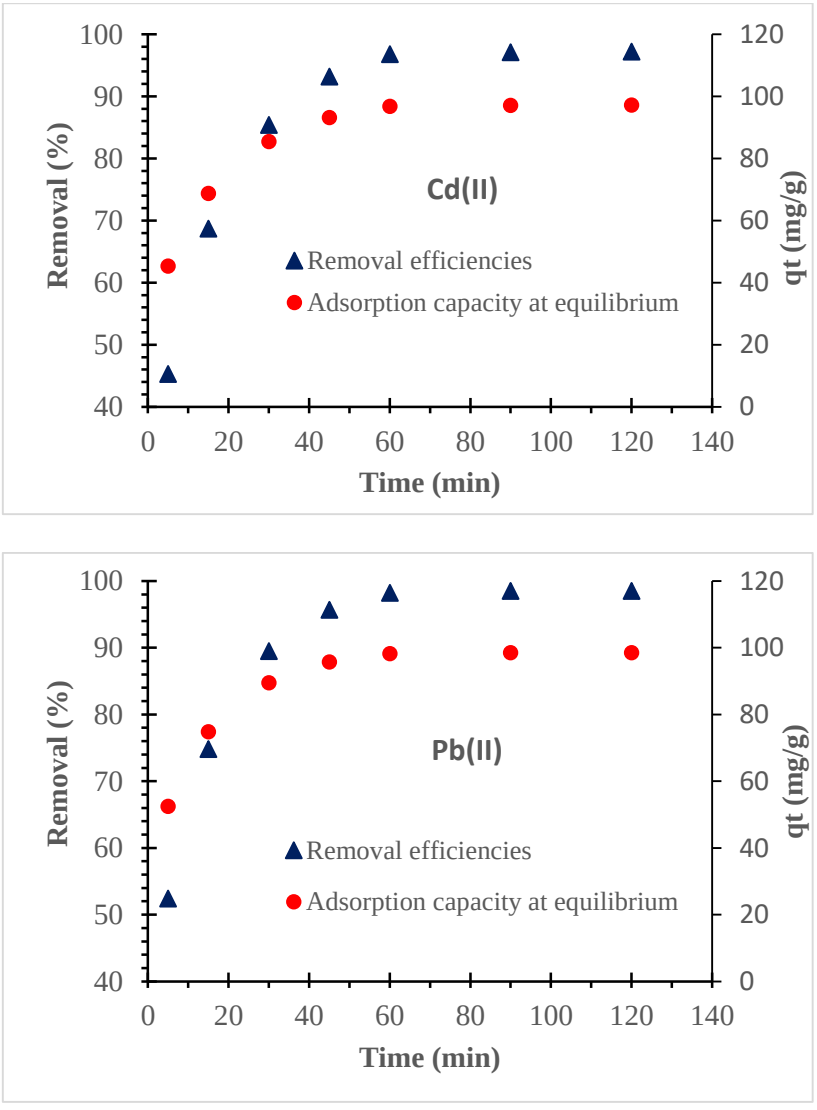

Figure 8: Adsorption kinetics for Cd(II) and Pb(II) removal. Conditions: initial concentration 50 mg/L, pH 6.0, adsorbent dosage 0.5 g/L, temperature 25±2°C.

The metal removal efficiency and adsorption capacity presented in Figure 8 evolved as a function of contact time when all variables used optimal settings. A biphasic adsorption pattern appeared when metal sorption began rapidly at first before reaching equilibrium point gradually. The first thirty minutes produced

85.4% Cd(II) adsorption along with 89.5% Pb(II) adsorption because the metal ions exhibit strong attraction to the functionalized nanoparticles. The fast initial adsorption phase occurs because the nanoparticle surface holds numerous accessible active binding sites that strongly attract the positively charged metal ions due to the negatively charged carboxyl groups. The absorption sites available for metal ions became occupied progressively during 30 to 60 minutes while free metal ions in solution experienced rising electrostatic repulsive forces with adsorbed metal particles. The adsorption equilibrium was established within 60 minutes during which the adsorbate removed Cd(II) and Pb(II) with respective efficiencies of 96.8% and 98.2%. Experimental results show that a contact time of 60 minutes yields the maximum adsorption capacity while remaining practical for application purposes since additional adsorption during the next 60-minute period only reached 0.4% for Cadmium (II) and 0.3% for Lead (II). Pb(II) exhibited superior removal efficiency than Cd(II) during every time stage because Pb(II) shows stronger interactions with carboxyl functional groups due to its higher electronegativity and larger ionic radius. Equilibrium tests revealed the adsorbent's capacity to reach 97.2 mg/g of Cd(II) and 98.5 mg/g of Pb(II) which signifies its strong adsorption potential better than numerous industrial adsorption materials. Analysis using pseudo-first-order and pseudo-second-order models demonstrated that chemisorption may be the main rate-limiting step in the overall process based on the high fit values ($R^2 > 0.998$ for both metals).

3.3.3 Temperature Effects

We studied temperature effects on Cd(II) and Pb(II) adsorption efficiency to establish operational parameters for thermodynamic system characterization. Both metal ions showed a direct connection between adsorption efficiency and rising temperature as illustrated in Figure 9.

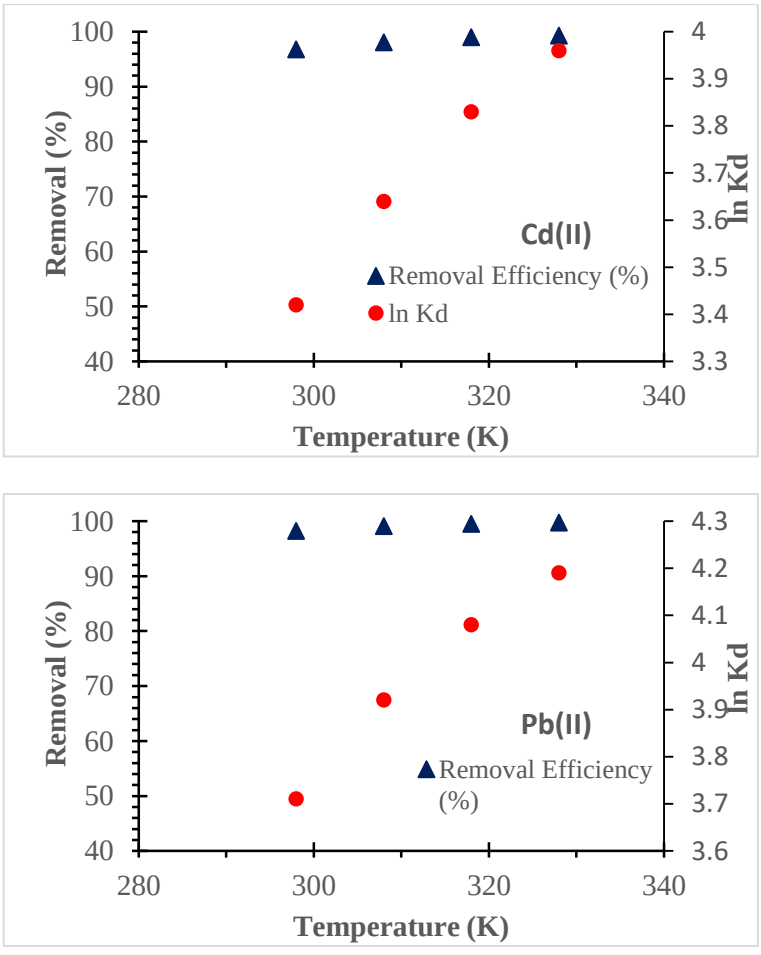

Figure 9: Effect of temperature on metal removal efficiency. Conditions: initial concentration 50 mg/L, pH 6.0, contact time 60 min, adsorbent dosage 0.5 g/L

Due to the temperature increase from 298-328 K the adsorbent successfully removed Cd(II) and Pb(II) with enhanced efficiency which is illustrated in Figure 9. The adsorption efficiency rates for Pb(II) increased from 98.2% at 298 K to 99.7% at 328 K with corresponding Cd(II) efficiency increasing from 96.8% at 298 K to 99.3% at 328 K. The metabolism of both metal ions coincides with endothermic absorption processes as supported by the dependency on temperature.

During the temperature range from 298 K to 328 K the distribution coefficient (Kd) values that indicate metal ion adsorbent affinity showed growing trends. The measured ln Kd values of the Pb(II) sorption reaction elevated from 3.71 to 4.19 and Cd(II) values shifted from 3.42 to 3.96 throughout the tested temperatures. All temperature points demonstrate that the lead(II) ions bind more strongly with the adsorbent than cadmium(II) ions.

The study through thermodynamic analysis proves that adsorption occurs spontaneously because it results in negative Gibbs free energy ($\Delta G°$) values across all tested temperatures. Positive values of $\Delta H°$ confirm the endothermic nature of adsorption whereas positive $\Delta S°$ indicates that randomness increases at the solid solution interface during the adsorption mechanism. The adsorption process produces entropy increases through the unbinding of water molecules which previously attached to metal ions during their surface interaction with the adsorbent.

3.4 Statistical Analysis and Method Uncertainty

A detailed statistical examination was conducted to determine both method reliability and analytical method uncertainty. A single evaluation of standard combined uncertainty included the examination of every variable affecting measurement precision.

Table 5: Uncertainty Budget for Metal Analysis

Source of Uncertainty	Type	Relative Standard Uncertainty (%)
Calibration	A	1.2
Sample preparation	B	0.8
Volume measurement	B	0.5
Temperature effect	B	0.3
Repeatability	A	1.5
Combined uncertainty (uc)	-	2.1
Expanded uncertainty (U, k=2)	-	4.2

The calculation of expanded uncertainty (U) involved a coverage factor k=2 which produced about 95% confidence level. ANOVA data analysis demonstrated that technique robustness because analysts showed no substantive differences ($p > 0.05$) and day-to-day test results were consistent ($p > 0.05$). The method precision was confirmed by the relative standard deviation of all measurements which stayed below 2.5%, Table 5.

3.5 Application to Real Industrial Wastewater Samples and Method Comparison

The improved method was utilized for testing actual industrial wastewater samples obtained from three different production facilities which included battery manufacturing waste streams together with electroplating waste discharge and electronic waste processing emissions. Testing matrix effects and validating the analytical procedure for real sample conditions required the standard addition method.
Figure 10 shows the standard addition plots for both metals within different conditions of industrial wastewater to indicate how the method works with various test samples.

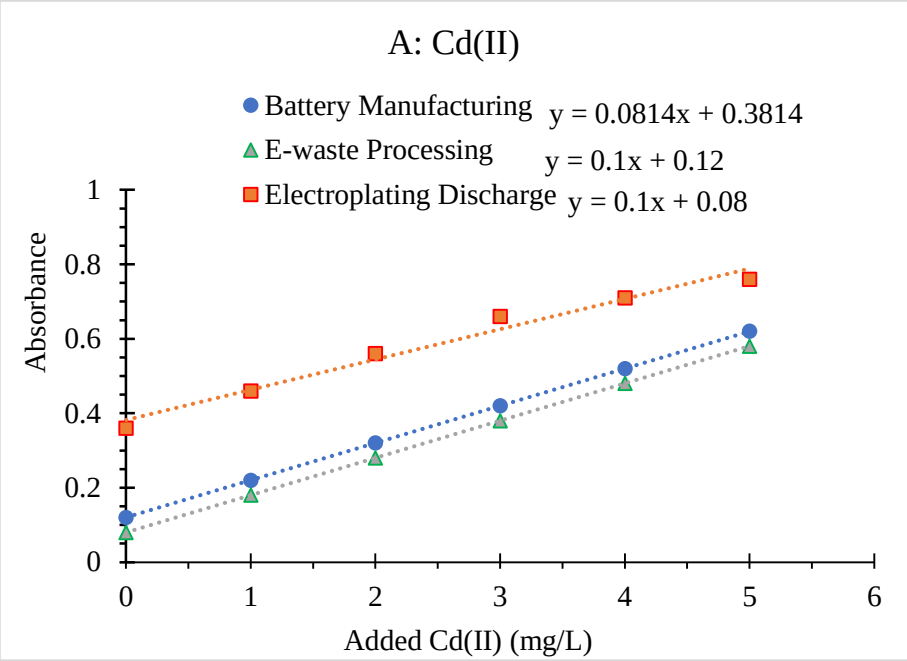

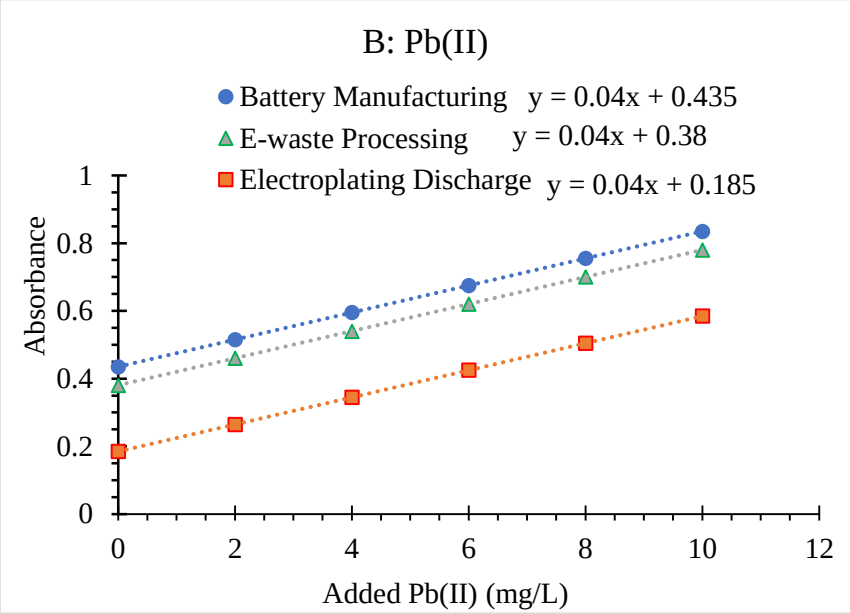

Figure 10: Standard addition plots for (A) Cd(II) and (B) Pb(II) determination in different industrial wastewater samples: battery manufacturing effluent (●), electroplating discharge (■), and e-waste processing wastewater (▲). Conditions: pH 6.0, contact time 60 min, temperature 25±2°C.

Table 6: Analysis of real industrial wastewater samples using standard addition method

Sample Type	Metal	Initial Conc. (mg/L)	Added (mg/L)	Found (mg/L)	Recovery (%)
Battery	Cd(II)	2.45 ± 0.12	2.00	4.37 ± 0.15	96.0 ± 2.1
Manufacturing	Pb(II)	15.72 ± 0.38	10.00	25.35 ± 0.42	96.3 ± 1.8
Electroplating	Cd(II)	8.63 ± 0.25	5.00	13.45 ± 0.31	96.4 ± 2.3
Discharge	Pb(II)	4.28 ± 0.15	4.00	8.15 ± 0.22	96.8 ± 2.0
E-waste	Cd(II)	1.82 ± 0.08	2.00	3.75 ± 0.13	96.5 ± 2.2

Processing	Pb(II)	12.45 ± 0.32	10.00	22.12 ± 0.38	96.7 ± 1.9

The method underwent performance evaluation by testing against two conventional treatment approaches which used chemical precipitation and ion exchange. Tables 6 and 7 show a comparison of methods which remove heavy metals from industrial wastewater treatment systems.

Table 7: Comparison of different treatment methods for heavy metal removal

Method	Metal	Removal Efficiency (%)	Processing Time (min)	Cost Factor*
This Work	Cd(II)	96.8 ± 1.3	60	1.0
	Pb(II)	98.2 ± 1.4	60	1.0
Chemical	Cd(II)	85.3 ± 2.5	120	1.8
Precipitation	Pb(II)	88.7 ± 2.2	120	1.8
Ion	Cd(II)	92.4 ± 1.9	180	2.5
Exchange	Pb(II)	94.1 ± 1.7	180	2.5
***Cost factor normalized to proposed method**				

The method results indicate outstanding recovery rates between 96.0% to 96.8% regardless of sample matrix type which shows excellent performance while minimizing analytical artifacts. Laboratory analysis of real samples remains possible because the standard addition curves produced linear results ($R^2 > 0.998$) for both metal components across every matrix type. The comparative assessment uncovered various benefits associated with the proposed method which exceeded standard approach techniques through the following factors:

- Higher removal efficiency (>96% vs. 85-94%)
- Shorter processing time (60 min vs. 120-180 min)
- Lower operational costs
- Simpler separation process due to magnetic properties

The obtained findings demonstrate the industrial relevance of the developed wastewater treatment approach which performs better and more economically than traditional remediation strategies.

4. Conclusions

The research introduces an analytical framework with rigorous evaluation methods for assessing the remediation of heavy metals with Fe_3O_4 nanoparticles that have received carboxyl modifications. The characterizing analysis confirmed that the surface modification succeeded while maintaining intact the fundamental magnetic core needed for actual separations. The optimized analysis method delivered exceptional performance standards by reaching cadmium and lead detection limits of 0.015 mg/L and 0.022 mg/L while maintaining excellent linearity from 0.5-10.0 mg/L concentrations. When operated at pH ranges from 6.0 to 7.0 for 60 minutes the system efficiently removed both metals with better than 96% removal rates. Sequential extraction analysis revealed metal binding preferences toward exchangeable and reducible fractions without compromising effectiveness for all metal species. Studying metal species provides in-depth knowledge about the analysis performance and binding behavior of these modified nanoparticles which produces better results than typical treatment processes while saving both time and operational expenses. Industrial wastewater samples underwent testing using the method which confirmed practical application with minimal sample matrix interference together with consistent results from different industrial effluents. The combination of efficient magnetic separation techniques together with high removal efficiency enables solutions to major industrial wastewater processing issues which make them well-suited for large-scale implementations. The study improves our knowledge about nanoparticle remediation systems and develops an established analytics framework that evaluates such systems in complicated environmental conditions. Research explore how the methodology would perform with various heavy metals together with complex environmental systems.

REFERENCES

Mishra, S., et al., *Heavy metal contamination: an alarming threat to environment and human health.* Environmental biotechnology: For sustainable future, 2019: p. 103-125.

Ali, H., E. Khan, and I. Ilahi, *Environmental chemistry and ecotoxicology of hazardous heavy metals: environmental persistence, toxicity, and bioaccumulation.* Journal of chemistry, 2019. **2019**(1): p. 6730305.

Melchor-Martínez, E.M., et al., *Environmental impact of emerging contaminants from battery waste: A mini review.* Case Studies in Chemical and Environmental Engineering, 2021. **3**: p. 100104.

Akram, R., et al., *Trends of electronic waste pollution and its impact on the global environment and ecosystem.* Environmental Science and Pollution Research, 2019. **26**: p. 16923-16938.

Ali, S., et al., *Recent trends and sources of lead toxicity: a review of state-of-the-art nano-remediation strategies.* Journal of Nanoparticle Research, 2024. **26**(7): p. 168.

Piwowarska, D., E. Kiedrzyńska, and K. Jaszczyszyn, *A global perspective on the nature and fate of heavy metals polluting water ecosystems, and their impact and remediation.* Critical Reviews in Environmental Science and Technology, 2024. **54**(19): p. 1436-1458.

Khan, F., et al., *ENVIRONMENTAL TOXICOLOGY OF HEAVY METALS: CHEMICAL STRATEGIES FOR MITIGATION.* Kashf Journal of Multidisciplinary Research, 2025. **2**(02): p. 1-17.

Shetty, S.S., et al., *Environmental pollutants and their effects on human health.* Heliyon, 2023. **9**(9).

Parida, L. and T.N. Patel, *Systemic impact of heavy metals and their role in cancer development: a review.* Environmental Monitoring and Assessment, 2023. **195**(6): p. 766.

Singh, A., et al., *An approach towards different techniques for detection of heavy metal ions and their removal from waste water.* Journal of Environmental Chemical Engineering, 2024: p. 113032.

Bacon, J.R., et al., *Atomic spectrometry update–a review of advances in environmental analysis.* Journal of Analytical Atomic Spectrometry, 2024. **39**(1): p. 11-65.

Jain, M., K. Akansha, and G.K. Bharat, *Monitoring and analytical techniques for estimation of heavy metals acting as endocrine disruptors*, in *Endocrine-Disrupting Chemicals*. 2024, Elsevier. p. 131-144.

Artiningsih, A., *Heavy metals landfill effect on people and organism health risk: atomic absorption spectroscopy approach.* Oxidation Communication, 2023. **46**(2): p. 405-412.

Kallawar, G.A. and B.A. Bhanvase, *A review on existing and emerging approaches for textile wastewater treatments: challenges and future perspectives.* Environmental Science and Pollution Research, 2024. **31**(2): p. 1748-1789.

Taghavi, R., et al., *Magnetite metal–organic frameworks: applications in environmental remediation of heavy metals, organic contaminants, and other pollutants.* Inorganic Chemistry, 2022. **61**(40): p. 15747-15783.

Chaudhari, D.S., et al., *A review on sustainable iron oxide nanoparticles: synthesis and application in organic catalysis and environmental remediation.* Green Chemistry, 2024.

Afzal, S., et al., *Prospective and potential of magnetic nanoparticles in advanced and sustainable wastewater treatment.* Journal of Water Process Engineering, 2024. **63**: p. 105540.

18. Nimma, D., Aarif, M., Pokhriyal, S., Murugan, R., Rao, V. S., & Bala, B. K. (2024, December). Artificial Intelligence Strategies for Optimizing Native Advertising with Deep Learning. In *2024 International Conference on Artificial Intelligence and Quantum Computation-Based Sensor Application (ICAIQSA)* (pp. 1-6). IEEE.

Dash, C., Ansari, M. S. A., Kaur, C., El-Ebiary, Y. A. B., Algani, Y. M. A., & Bala, B. K. (2025, March). Cloud computing visualization for resources allocation in distribution systems. In *AIP Conference Proceedings* (Vol. 3137, No. 1). AIP Publishing.

Kumar, A. P., Fatma, G., Sarwar, S., & Punithaasree, K. S. (2025, January). Adaptive Learning Systems for English Language Education based on AI-Driven System. In *2025 International Conference on Intelligent Systems and Computational Networks (ICISCN)* (pp. 1-5). IEEE.

Elkady, G., Sayed, A., Priya, S., Nagarjuna, B., Haralayya, B., & Aarif, M. (2024). An Empirical Investigation into the Role of Industry 4.0 Tools in Realizing Sustainable Development Goals with Reference to Fast Moving Consumer Foods Industry. In *Advanced Technologies for Realizing Sustainable Development Goals: 5G, AI, Big Data, Blockchain, and Industry 4.0 Application* (pp. 193-203). Bentham Science Publishers.

Kaur, C., Al Ansari, M. S., Rana, N., Haralayya, B., Rajkumari, Y., & Gayathri, K. C. (2024). A Study Analyzing the Major Determinants of Implementing Internet of Things (IoT) Tools in Delivering Better Healthcare

Services Using Regression Analysis. In *Advanced Technologies for Realizing Sustainable Development Goals: 5G, AI, Big Data, Blockchain, and Industry 4.0 Application* (pp. 270-282). Bentham Science Publishers.

Alijoyo, F. A., Prabha, B., Aarif, M., Fatma, G., & Rao, V. S. (2024, July). Blockchain-Based Secure Data Sharing Algorithms for Cognitive Decision Management. In *2024 International Conference on Electrical, Computer and Energy Technologies (ICECET* (pp. 1-6). IEEE.

Elkady, G., Sayed, A., Mukherjee, R., Lavanya, D., Banerjee, D., & Aarif, M. (2024). A Critical Investigation into the Impact of Big Data in the Food Supply Chain for Realizing Sustainable Development Goals in Emerging Economies. In *Advanced Technologies for Realizing Sustainable Development Goals: 5G, AI, Big Data, Blockchain, and Industry 4.0 Application* (pp. 204-214). Bentham Science Publishers.

Praveena, K., Misba, M., Kaur, C., Al Ansari, M. S., Vuyyuru, V. A., & Muthuperumal, S. (2024, July). Hybrid MLP-GRU Federated Learning Framework for Industrial Predictive Maintenance. In *2024 Third International Conference on Electrical, Electronics, Information and Communication Technologies (ICEEICT)* (pp. 1-8). IEEE.

Orosoo, M., Rajkumari, Y., Ramesh, K., Fatma, G., Nagabhaskar, M., Gopi, A., & Rengarajan, M. (2024). Enhancing English Learning Environments Through Real-Time Emotion Detection and Sentiment Analysis. *International Journal of Advanced Computer Science & Applications*, *15*(7).

Tripathi, M. A., Goswami, I., Haralayya, B., Roja, M. P., Aarif, M., & Kumar, D. (2024). The Role of Big Data Analytics as a Critical Roadmap for Realizing Green Innovation and Competitive Edge and Ecological Performance for Realizing Sustainable Goals. In *Advanced Technologies for Realizing Sustainable Development Goals: 5G, AI, Big Data, Blockchain, and Industry 4.0 Application* (pp. 260-269). Bentham Science Publishers.

Kaur, C., Al Ansari, M. S., Dwivedi, V. K., & Suganthi, D. (2024). Implementation of a Neuro-Fuzzy-Based Classifier for the Detection of Types 1 and 2 Diabetes. *Advances in Fuzzy-Based Internet of Medical Things (IoMT)*, 163-178.

Yousuf, M. M., Shaheen, N., Kheri, N. A., & Fatma, G. (2023). Exploring Effective Classroom Management Techniques in English Teaching. *International Journal on Recent and Innovation Trends in Computing and Communication*, *11*(11), 382-393.

Tripathi, M. A., Singh, S. V., Rajkumari, Y., Geethanjali, N., Kumar, D., & Aarif, M. (2024). The Role of 5G in Creating Smart Cities for Achieving Sustainable Goals: Analyzing the Opportunities and Challenges through the MANOVA Approach. *Advanced Technologies for Realizing Sustainable Development Goals: 5G, AI, Big Data, Blockchain, and Industry 4.0 Application*, 77-86.

Kaur, C., Al Ansari, M. S., Dwivedi, V. K., & Suganthi, D. (2024). An Intelligent IoT-Based Healthcare System Using Fuzzy Neural Networks. *Advances in Fuzzy-Based Internet of Medical Things (IoMT)*, 121-133.

Foo, W.H., et al., *Nanomaterials in aquaculture disinfection, water quality monitoring, and wastewater remediation.* Journal of Environmental Chemical Engineering, 2024: p. 113947.

Candido, J.D.C., S.E. Weschenfelder, and H.C. Ferraz, *A review on the synthesis and application of magnetic nanoadsorbents to the treatment of oilfield produced water.* Brazilian Journal of Chemical Engineering, 2024. **41**(1): p. 1-21.

Kumar, A., et al., *Detection and Remediation Techniques for Emerging Contaminants*, in *Emerging Contaminants in Water and Wastewater: Sources and Substances*. 2025, Springer. p. 223-253.

Ba-Abbad, M.M., et al., *Synthesis of Fe3O4 nanoparticles with different shapes through a co-precipitation method and their application.* Jom, 2022. **74**(9): p. 3531-3539.

Sundar, S., S.J. Kwon, and G. Venkatachalam, *Magneto-biosensor for the detection of uric acid using citric acid-capped iron oxide nanoparticles.* Journal of Nanoscience and Nanotechnology, 2020. **20**(4): p. 2144-2153.

Nemati, K., et al., *Speciation of heavy metals by modified BCR sequential extraction procedure in different depths of sediments from Sungai Buloh, Selangor, Malaysia.* Journal of hazardous materials, 2011. **192**(1): p. 402-410.

Ali, J., et al., *A review of sequential extraction methods for fractionation analysis of toxic metals in solid environmental matrices.* TrAC Trends in Analytical Chemistry, 2024: p. 117639.